Birth of periodic and artificial halo orbits in the restricted three-body problem

Marta Ceccaroni[1]

Department of Mathematics, University of Roma Tor Vergata,
Via della Ricerca Scientifica, 1 - 00133 Roma

Alessandra Celletti[2]

Department of Mathematics, University of Roma Tor Vergata,
Via della Ricerca Scientifica 1, 00133 Roma (Italy)

Giuseppe Pucacco[3]

Department of Physics, University of Roma Tor Vergata,
Via della Ricerca Scientifica 1, 00133 Roma (Italy)

Keywords: Three–body problem, Collinear points, Halo orbits, Bifurcation theory, Solar radiation pressure.

---

[1]ceccaron@mat.uniroma2.it
[2]celletti@mat.uniroma2.it
[3]pucacco@roma2.infn.it; telephone/fax: +39 06 72594541.

Preprint submitted to *September 19, 2015*

Birth of periodic and artificial halo orbits in the restricted three-body problem

Marta Ceccaroni[1]

Department of Mathematics, University of Roma Tor Vergata, Via della Ricerca Scientifica, 1 - 00133 Roma

Alessandra Celletti[2]

Department of Mathematics, University of Roma Tor Vergata, Via della Ricerca Scientifica 1, 00133 Roma (Italy)

Giuseppe Pucacco[3]

Department of Physics, University of Roma Tor Vergata, Via della Ricerca Scientifica 1, 00133 Roma (Italy)

Abstract

We investigate the bifurcation of artificial halo orbits from the Lyapunov planar family of periodic orbits around the collinear libration points of the circular, spatial, restricted three–body problem. Beside the gravitational forces, our model includes also the effect of the Solar Radiation Pressure (SRP) and this motivates the use of the term 'artificial' halo orbits. Indeed, as a typical problem, one may think of a solar sail, which is characterized by a performance parameter measuring the strength of the effect of the SRP on the spacecraft.

To settle the model, we determine the position of the collinear points as a function of the mass and performance parameters and the energy values at which Hill's surfaces allow for transit orbits between the primaries. To analyze the dynamics we use a consolidated procedure which consists in the computation of a resonant normal form, allowing the reduction to the center manifold and providing an integrable approximation of the Hamiltonian dynamical system. Finally, we compute the bifurcation thresholds of the 1:1 resonant periodic orbit families (which have the standard 'halo' orbits as their first member) as a function of the performance and mass parameters.

The results show that SRP is indeed a relevant ingredient for new dynamical features and must definitely be considered when planning a mission of a solar sail with trajectories in the neighborhoods of collinear points.

---

[1]ceccaron@mat.uniroma2.it
[2]celletti@mat.uniroma2.it
[3]pucacco@roma2.infn.it; telephone/fax: +39 06 72594541.

1. Introduction

Since the works of Euler ([6]) and Lagrange ([12]), it is known that the restricted three-body problem admits five equilibrium points in the synodical reference frame (namely, a frame rotating with the angular velocity of the primaries). Three of such equilibrium positions, named the *collinear* equilibria, are located along the line joining the primaries and are shown to be unstable, while the other two equilibria, called *triangular* positions, are stable provided the mass ratio of the primaries is lower than a given threshold (see, e.g., [15]).

The aim of this work is to investigate the effect of the Solar Radiation Pressure (SRP hereinafter) on the existence of periodic orbits around the collinear libration points of the circular, spatial, restricted three–body problem, and precisely the 1:1 resonant periodic orbit families (which have the standard so–called *halo* orbits as their first member). These orbits are three-dimensional periodic trajectories resulting from the interaction between the gravitational pull of two planetary bodies, and the Coriolis and centrifugal accelerations acting on the spacecraft. They bifurcate/annihilate from/to the Lyapunov orbits with bifurcation sequences parametrised by the energy with thresholds determined by the two relevant parameters of the model, the mass-ratio of the primaries μ and the SRP performance parameter β.

The dynamics around the collinear points has gained an increasing interest in the space era. Since then, several space missions have fully exploited the capabilities of such equilibrium positions. Furthermore, it was suggested to use the Earth–Moon L_2 halo orbit as a communication relay station for an Apollo mission to the far side of the Moon, as it would enable continuous views of both the Earth and the hidden Moon. Yet, the establishment of a bridge for radio communication is a significant problem for future space missions, planning to use the outer side of the Moon as a launch site for space explorations or as an observation point.

Moreover, a number of missions have used the Sun-Earth L_1 halo orbits, like the International Sun-Earth Explorer (ISEE-3 1978), the Solar and Heliospheric Observatory (SOHO 1996) and Genesis (2001). All these space missions have a strategic importance for solar-wind physics, cosmic-ray physics, and astrophysics. Remarkably, the Next Generation Space Telescope (NGST) and Lisa Pathfinder will also use halo orbits.

There are extensive results in the literature about the determination of accurate approximations of such equilibrium orbits. Just to quote some results, in 1973 Hénon [10] studied the stability of the planar Lyapunov orbits with respect to vertical perturbations, see also [16]. A center manifold reduction was used by Barden and Howell [1], Jorba and Masdemont [11] and Gomez and Mondelo [9] in combination with the Lindstedt-Poincaré method, which enabled them to develop a semi-analytical technique to describe and compute solutions in the extended neighborhood of an equilibrium point. A method for the analytic evaluation of the bifurcation thresholds in terms of the energy in the rotating frame has been progressively illustrated in [5], [2], [3], the latter work showing a good agreement with the numerical results found in the literature.

Using the same methodology developed in the above mentioned works, this paper extends the results to the case accounting for the effect of SRP into the model. The effect of SRP implies that the position of the collinear points will be slightly modified. In addition, Hill's regions are altered by the SRP (compare with Section 2). As it is well known, there exists an energy range in which the region of admissible motion is confined around each primary, preventing transfers between them. By modifying the energy, it is possible to open the gates at the Lagrangian points L_1, L_2 and L_3 in sequence, thus enabling transit and escape orbits, respectively. The effect of the SRP will be to lower the energy threshold at which the gates open, when compared with the model without SRP. The study of the location of the collinear points as well as of the corresponding Hill's regions will be performed, for completeness, for all three collinear points, although the analysis of the bifurcation thresholds will be limited to L_1 and L_2, since the equilibrium point L_3 has no relevant applications in space dynamics; furthermore, it has been shown in [3] that the normal form is not a reliable technique for L_3, when the mass ratio of the primaries is smaller than 10^{-2}, since the optimal order of expansion is very low (see [3] for full details).

Thus, limiting ourselves to L_1 and L_2, we show that exploiting SRP with the use of a reflecting device, e.g. a solar sail, it is possible to get a change of the energy thresholds at which halo orbits and other periodic orbits take place in the vicinities of L_1 and L_2. The results show that SRP significantly affects the energy needed for the bifurcations of the periodic orbits, especially for low mass ratios. Moreover, we provide the thresholds for the bifurcations of other families of periodic orbits, and their behavior as a function of the mass and sail parameters. Indeed, around the equilibria, SRP enables bifurcations of other families of periodic orbits, lowering their bifurcation thresholds to conceivable and reachable values.

This paper is organized as follows. Section 2 provides the equations describing the dynamics of the spatial, circular, restricted three–body problem (hereafter, SCR3BP) with solar radiation pressure. Moreover, we describe a procedure to derive an explicit formulation for the position of the collinear equilibria in terms of the mass and solar sail parameters. Finally, we compare the energies of the zero–velocity curves for the cases with and without SRP. Section 3 provides the fundamental steps to reduce the Hamiltonian to the center manifold; however, since the procedure has been inherited by previous works, only the main steps are hereby described. The values for the bifurcation of the resonant periodic orbits with SRP around L_1 and L_2 are derived in Section 4, where the behavior of the thresholds is analyzed in terms of the mass parameter, and for a range of physically relevant values of the performance parameter. Some conclusions are given in Section 5.

2. Collinear points in the three-body problem with SRP

In this Section we introduce the equations of motion describing the SCR3BP and we present a model including the effect of solar radiation pressure. Within such framework we determine the position of the collinear equilibria, taking care of the dependance of their position upon the mass ratio of the primaries and the *solar sail* performance parameter (namely, the SRP parameter). A first analysis of the energy levels characterising the system is carried on using the zero-velocity curves. These curves first confine the admissible motion around the primaries (or in the outer space), then, increasing the energy, first allow the planetary interchange orbits and then escape through L_2 and L_3. In particular, we study the dependence of such energy levels on the SRP parameter. As we mentioned in Section 1, we will discuss all three collinear points, although in Section 4 the discussion will be limited to L_1 and L_2.

2.1. The model

We consider the dynamics of a massless body, moving under the gravitational attraction of two massive bodies, say P_1, P_2, called the primaries. We assume that the primaries move on circular orbits with constant angular velocity around their common center of mass. The biggest primary is supposed to be a radiating body, while the massless body is assumed to be a perfectly reflecting solar sail (see, e.g., [14]), which is characterized by a *performance parameter*, say β, defined as

$$\beta \equiv \frac{L_\odot Q}{4\pi c \; G M_\odot B} \ . \tag{1}$$

The quantities appearing in (1) have the following meaning: $L_\odot = 3.839 \times 10^{26}$ $Watt$ is the Sun's luminosity, $Q \equiv 1 + c_R$ where c_R is the reflectivity coefficient of the sail, c is the speed of light, G is the gravitational constant, $M_\odot$ is the mass of the Sun and $B = m/\mathcal{A}$ is the mass-to-area ratio of the spacecraft (m is the mass and $\mathcal{A}$ is the area of the spacecraft). We refer to [8] for a model encompassing a non–perfectly reflecting sail.

We consider a synodic reference frame (O, X, Y, Z) with origin O located in the center of mass of the two primaries; the frame rotates with their angular velocity, so that the positions of the primaries are fixed on the X axis, the Y axis belongs to the plane of motion of the primaries and the Z axis forms a clockwise oriented frame.

We scale the units of measure such that the sum of the masses of the primaries, their distance and the angular velocity is set to unity. Let μ and $1-\mu$ be the scaled masses of the primaries with $\mu \in (0, 1/2]$. Then, the position of the smaller primary is at $(-1+\mu, 0, 0)$, while the larger primary is located at $(\mu, 0, 0)$. With such convention L_2 is at the left of the smaller primary, L_1 is between the primaries and L_3 is located at the right of the larger primary.

Let (X, Y, Z) be the coordinates of the third body in the synodic reference frame and let (P_X, P_Y, P_Z) be the conjugated kinetic momenta defined as $P_X = \dot{X} - Y$, $P_Y = \dot{Y} + X$, $P_Z = \dot{Z}$. We assume that the solar sail is perpendicular to the Sun–sail direction; notice that this assumption ensures the Hamiltonian character of the model. We refer to [7] for different models in which the orientation of the sail is varied.

With these notations and settings, the equations of motion are given by

$$\begin{aligned} \ddot{X} - 2\dot{Y} &= \frac{\partial \Omega}{\partial X} \\ \ddot{Y} + 2\dot{X} &= \frac{\partial \Omega}{\partial Y} \\ \ddot{Z} &= \frac{\partial \Omega}{\partial Z} , \end{aligned} \tag{2}$$

where we introduced the *pseudo-potential* $\Omega = \Omega(X, Y, Z)$ as

$$\Omega(X, Y, Z) \equiv \frac{1}{2}(X^2 + Y^2) + \frac{(1-\beta)(1-\mu)}{r_1} + \frac{\mu}{r_2} \tag{3}$$

with

$$r_1 = \sqrt{(X-\mu)^2 + Y^2 + Z^2} , \qquad r_2 = \sqrt{(X-\mu+1)^2 + Y^2 + Z^2} \tag{4}$$

(see [2]).

The equations (2) are associated to the following Hamiltonian function:

$$\begin{aligned} H^{(IN)}(P_X, P_Y, P_Z, X, Y, Z) &= \frac{1}{2}(P_X^2 + P_Y^2 + P_Z^2) + YP_X - XP_Y \\ &- \frac{(1-\beta)(1-\mu)}{r_1} - \frac{\mu}{r_2} . \end{aligned} \tag{5}$$

Provided that the mass parameter μ satisfies some conditions now depending also on β, the system of equations (2) admits five equilibrium positions, which are found as the solutions of the system of equations:

$$\frac{\partial \Omega}{\partial X} = 0 , \qquad \frac{\partial \Omega}{\partial Y} = 0 , \qquad \frac{\partial \Omega}{\partial Z} = 0 .$$

All five equilibria lie on the plane $Z = 0$. We stress that in the next Sections we will just consider the dynamics of the collinear equilibria L_1, L_2, L_3, whose location will be computed in Section 2.2.

2.2. The location of the collinear equilibria under SRP

In this Section we describe the procedure to derive an explicit formulation for the position of the equilibria in terms of the mass parameter μ and the sail parameter β.
For the case $\beta = 0$ the dependence of the equilibria upon the mass parameter is provided e.g. in [15]. In this Section this computation is extended to the case with solar radiation pressure, the main difference being that in the perturbed case the solutions must be expanded around the unperturbed solution found for the case with $\beta = 0$.

Using (4) and recalling that we consider the planar equilibria with $Z = 0$, we obtain

$$(1-\mu)r_1^2 + \mu r_2^2 = X^2 + Y^2 + (1-\mu)\mu \ .$$

The pseudo-potential (3) can therefore be written as

$$\Omega = (1-\mu)\left(\frac{r_1^2}{2} + \frac{(1-\beta)}{r_1}\right) + \mu\left(\frac{r_2^2}{2} + \frac{1}{r_2}\right) - \frac{1}{2}(1-\mu)\mu \ . \qquad (6)$$

Therefore, the equilibria of the model are given by the solutions of the following equations:

$$\begin{aligned}
\frac{\partial\Omega}{\partial X} &= (1-\mu)\left(r_1 - \frac{(1-\beta)}{r_1^2}\right)\left(\frac{X-\mu}{r_1}\right) + \mu\left(r_2 - \frac{1}{r_2^2}\right)\left(\frac{X+1-\mu}{r_2}\right) = 0 \\
\frac{\partial\Omega}{\partial Y} &= (1-\mu)\left(r_1 - \frac{(1-\beta)}{r_1^2}\right)\left(\frac{Y}{r_1}\right) + \mu\left(r_2 - \frac{1}{r_2^2}\right)\left(\frac{Y}{r_2}\right) = 0 \ .
\end{aligned}$$

In passing by, we notice that the two triangular solutions are obtained by solving the equations

$$r_1 - \frac{(1-\beta)}{r_1^2} = 0 \ , \qquad r_2 - \frac{1}{r_2^2} = 0 \ ,$$

which give the two equilibrium positions $L_4 = (x_e, y_e^-)$ and $L_5 = (x_e, y_e^+)$ with

$$\begin{aligned}
x_e &= -\frac{(1-\beta)^{\frac{2}{3}}}{2} + \mu \\
y_e^{\pm} &= \pm\frac{|(1-\beta)|^{\frac{1}{3}}}{2}\sqrt{4-(1-\beta)^{\frac{2}{3}}} \ .
\end{aligned}$$

As for the collinear equilibria it is first stressed that, for $Y = Z = 0$ and calling γ the distance of the equilibria from the closer primary, the distances

r_1, r_2 are given for L_1, L_2, L_3 by the following relations:

$$\begin{array}{llcl} L_1: & r_1 & = & |X-\mu| = -(X-\mu) = 1-\gamma \ , \\ & r_2 & = & |X-\mu+1| = X-\mu+1 = \gamma \\ L_2: & r_1 & = & |X-\mu| = -(X-\mu) = 1+\gamma \ , \\ & r_2 & = & |X-\mu+1| = -(X-\mu+1) = \gamma \\ L_3: & r_1 & = & |X-\mu| = X-\mu = \gamma \ , \\ & r_2 & = & |X-\mu+1| = X-\mu+1 = 1+\gamma \ . \end{array} \tag{7}$$

From the above expressions we obtain that the quantity γ is given by the solution of the following equations:

$$\begin{array}{ll} L_1: & -(1-\mu)\left(1-\gamma-\dfrac{(1-\beta)}{(1-\gamma)^2}\right)+\mu\left(\gamma-\dfrac{1}{\gamma^2}\right)=0 \\ L_2: & -(1-\mu)\left(1+\gamma-\dfrac{(1-\beta)}{(1+\gamma)^2}\right)-\mu\left(\gamma-\dfrac{1}{\gamma^2}\right)=0 \\ L_3: & (1-\mu)\left(\gamma-\dfrac{(1-\beta)}{\gamma^2}\right)+\mu\left((1+\gamma)-\dfrac{1}{(1+\gamma)^2}\right)=0 \ , \end{array}$$

which can be written as

$$\begin{array}{ll} L_1: & \dfrac{-1+\gamma+\frac{(1-\beta)}{(-1+\gamma)^2}}{3\left(-\gamma+\frac{1}{\gamma^2}\right)} = \dfrac{\mu}{3(1-\mu)} \\ L_2: & \dfrac{-1-\gamma+\frac{(1-\beta)}{(1+\gamma)^2}}{3\left(\gamma-\frac{1}{\gamma^2}\right)} = \dfrac{\mu}{3(1-\mu)} \\ L_3: & \dfrac{\gamma-\frac{(1-\beta)}{\gamma^2}}{3\left(-(1+\gamma)+\frac{1}{(1+\gamma)^2}\right)} = \dfrac{\mu}{3(1-\mu)} \ . \end{array}$$

We proceed now to find the solution for the case $\beta = 0$, which will be needed for developing the result of the general case with $\beta \neq 0$. According to a standard procedure (see, e.g., [4]), setting $\beta = 0$ and defining $\alpha = \left(\frac{\mu}{3(1-\mu)}\right)^{\frac{1}{3}}$, we start by expanding α as a function of μ in Taylor series up to order four; the expansion is performed around $\mu = 0$ for L_1, L_2, and around $\mu = 1$ for L_3. Afterwards, we proceed to invert such relations, thus finding the distances of the case $\beta = 0$, say $\gamma_i = \bar{\gamma}_i$, $i = 1, 2, 3$, in series of μ.

For the case $\beta \neq 0$ we start by expanding α in Taylor series around the values $\bar{\gamma}_i$, $i = 1, 2, 3$, computed for $\beta = 0$; then, we invert such relations to find the distances γ_i, $i = 1, 2, 3$, in series of μ. The result of this procedure is given by the following relations:

$$
\begin{aligned}
\gamma_1 = & \frac{\bar\gamma_1(\mathcal{F}_1(\beta(-1+2\bar\gamma_1+2\bar\gamma_1^2+6\bar\gamma_1^3)-\bar\gamma_1^2(3+2\bar\gamma_1+11\bar\gamma_1^2-10\bar\gamma_1^3+3\bar\gamma_1^4)))}{\mathcal{F}_1(\beta(2+2\bar\gamma_1+2\bar\gamma_1^2+3\bar\gamma_1^3)+\bar\gamma_1(-9+6\bar\gamma_1-5\bar\gamma_1^2-2\bar\gamma_1^3+\bar\gamma_1^4))} \\
& + \frac{\bar\gamma_1(3(-1+\bar\gamma_1^3)(-\beta+\bar\gamma_1(3-3\bar\gamma_1+\bar\gamma_1^2))(-\frac{\mu}{(-1+\mu)})^{\frac{1}{3}})}{\mathcal{F}_1(\beta(2+2\bar\gamma_1+2\bar\gamma_1^2+3\bar\gamma_1^3)+\bar\gamma_1(-9+6\bar\gamma_1-5\bar\gamma_1^2-2\bar\gamma_1^3+\bar\gamma_1^4))}
\end{aligned} \tag{8}
$$

$$
\begin{aligned}
\gamma_2 = & \frac{\bar\gamma_2(\mathcal{F}_2(\beta(-1-3\bar\gamma_2+4\bar\gamma_2^3+6\bar\gamma_2^4)+\bar\gamma_2^2(-3-\bar\gamma_2+9\bar\gamma_2^2+21\bar\gamma_2^3+13\bar\gamma_2^4+3\bar\gamma_2^5)))}{\mathcal{F}_2(\beta(2+\bar\gamma_2^3+3\bar\gamma_2^4)+\bar\gamma_2(9+15\bar\gamma_2+11\bar\gamma_2^2+3\bar\gamma_2^3+3\bar\gamma_2^4+\bar\gamma_2^5))} \\
& + \frac{\bar\gamma_2(-3(-1-\bar\gamma_2+\bar\gamma_2^3+\bar\gamma_2^4)(\beta+\ \bar\gamma_2(3+3\bar\gamma_2+\bar\gamma_2^2))(-\frac{\mu}{(-1+\mu)})^{\frac{1}{3}})}{\mathcal{F}_2(\beta(2+\bar\gamma_2^3+3\bar\gamma_2^4)+\bar\gamma_2(9+15\bar\gamma_2+11\bar\gamma_2^2+3\bar\gamma_2^3+3\bar\gamma_2^4+\bar\gamma_2^5))}
\end{aligned} \tag{9}
$$

$$
\begin{aligned}
\gamma_3 = & \frac{\bar\gamma_3(-\mathcal{F}_3(-18-33\bar\gamma_3-23\bar\gamma_3^2+3\bar\gamma_3^3+15\bar\gamma_3^4+11\bar\gamma_3^5+3\bar\gamma_3^6+\beta(18+33\bar\gamma_3+23\bar\gamma_3^2+6\bar\gamma_3^3)))}{\mathcal{F}_3(9+15\bar\gamma_3+11\bar\gamma_3^2+3\bar\gamma_3^3+3\bar\gamma_3^4+\bar\gamma_3^5-\beta(9+15\bar\gamma_3+11\bar\gamma_3^2+3\bar\gamma_3^3))} \\
& + \frac{\bar\gamma_3(3(-1+\beta+\bar\gamma_3^3)(3+6\bar\gamma_3+4\bar\gamma_3^2+\bar\gamma_3^3)(-\frac{\mu}{(-1+\mu)})^{\frac{1}{3}})}{\mathcal{F}_3(9+15\bar\gamma_3+11\bar\gamma_3^2+3\bar\gamma_3^3+3\bar\gamma_3^4+\bar\gamma_3^5-\beta(9+15\bar\gamma_3+11\bar\gamma_3^2+3\bar\gamma_3^3))} \ ,
\end{aligned} \tag{10}
$$

where the quantities $\mathcal{F}_1$, $\mathcal{F}_2$, $\mathcal{F}_3$ are given by the following expressions:

$$
\begin{aligned}
\mathcal{F}_1 &= \left(\frac{\bar\gamma_1^2(\beta-\bar\gamma_1(3-3\bar\gamma_1+\bar\gamma_1^2))}{(-1+\bar\gamma_1)^3(1+\bar\gamma_1+\bar\gamma_1^2)}\right)^{\frac{1}{3}} \\
\mathcal{F}_2 &= \left(-\frac{(\bar\gamma_2^2(\beta+\bar\gamma_2(3+3\bar\gamma_2+\bar\gamma_2^2)))}{(1+\bar\gamma_2)^2(-1+\bar\gamma_2^3)}\right)^{\frac{1}{3}} \\
\mathcal{F}_3 &= \left(-\frac{(1+\bar\gamma_3)^2(-1+\beta+\bar\gamma_3^3)}{\bar\gamma_3^3(3+3\bar\gamma_3+\bar\gamma_3^2)}\right)^{\frac{1}{3}} \ .
\end{aligned}
$$

We stress that the analytical expressions (8), (9), (10), for the γ_i, $i=1,2,3$, will be needed to evaluate the energy levels which allow for transit orbits between the primaries, as performed in Section 2.3.

The comparison between the results provided by the analytical formulas (8), (9), (10), and the values obtained numerically is shown in Figure 1. Such Figure also shows the difference of the results between the cases $\beta=0$ and $\beta\neq 0$.

2.3. Zero–velocity curves with SRP

It is well known that the system of equations (2) admits as an integral of motion the so-called *Jacobi energy*, defined by

$$
\mathcal{J}(\dot X,\dot Y,\dot Z,X,Y,Z) = -(\dot X^2+\dot Y^2+\dot Z^2)+2\Omega(X,Y,Z)
$$

with Ω as in (6). Therefore, for a fixed energy level E, we obtain that the subset of the phase space defined as

$$
\mathcal{L}(E) = \Big\{(X,Y,Z,\dot X,\dot Y,\dot Z)\in\mathbb{R}^6:\ \mathcal{J}=E,\ E\in\mathbb{R}\Big\}
$$

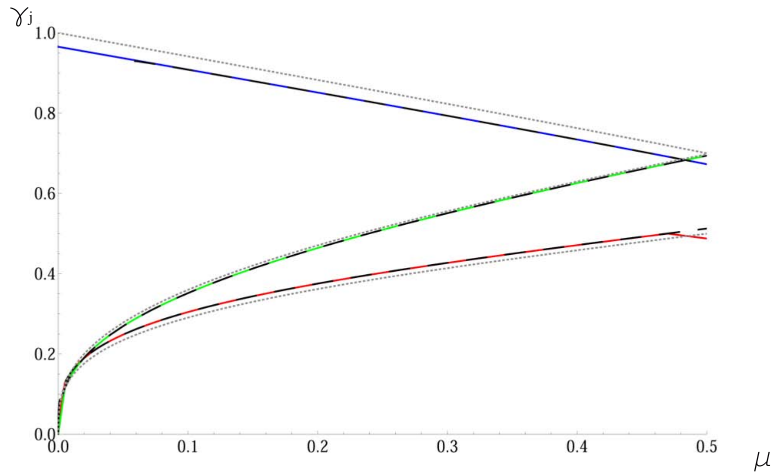

Figure 1: The values γ_i, $i = 1, 2, 3$, evaluated numerically (continuous, coloured lines, for L_1, L_2, L_3 in red, green, blue, respectively) and the values γ_i, $i = 1, 2, 3$, found using the expansions (8), (9), (10) (dashed, black lines - nearly overlapping with the coloured lines); the parameter β has been set to $\beta = 0.1$. The dotted lines provide the values $\bar{\gamma}_i$ corresponding to the case $\beta = 0$.

is a three dimensional manifold for which the solutions of (2) which start on $\mathcal{L}(E)$ will remain on it for all times.

The projections of the manifold $\mathcal{L}(E)$ taking a section with $Z = 0$ onto the (X, Y)-plane and setting $\dot{X} = \dot{Y} = \dot{Z} = 0$ provide the *zero-velocity* curves, which delimitate the so-called *Hill's regions*, defined as

$$\mathcal{H}(E) = \left\{(X, Y) \in \mathbb{R}^2 : \ 2\Omega(X, Y, 0) - E \geq 0\right\} \ . \tag{11}$$

For a given energy level, the boundaries of (11) confine the motion of the spacecraft in specific domains, which could be around one of the primaries without exchange or escape possibilities, or rather with transfer between primaries but still without escape up to the free motion in the whole space.

Substituting (8), (9) or (10) into (6) will thus provide the values E_1, E_2 and E_3 for the Jacobi constant at the three equilibria, respectively. Recalling (7), the results in terms of the mass and sail parameters are given by

$$\begin{aligned}
E_1 &= -[-\gamma_1^4 + \gamma_1^3(3 - 2\mu) + 2\mu + \gamma_1(3 + 2\beta(-1 + \mu) - 4\mu - \mu^2) \\
&+ \gamma_1^2(-3 + 2\mu + \mu^2)]/[2(-1 + \gamma_1)\gamma_1] \\
E_2 &= -(3\gamma_2 - 2\beta\gamma_2 + 3\gamma_2^2 + 3\gamma_2^3 + \gamma_2^4 + 2\mu + 2\beta\gamma_2\mu - 2\gamma_2^2\mu \\
&- 2\gamma_2^3\mu - \gamma_2\mu^2 - \gamma_2^2\mu^2)/[2\gamma_2(1 + \gamma_2)] \\
E_3 &= [\gamma_3^4 + 2(-1 + \mu) - 2\beta(1 + \gamma_3)(-1 + \mu) + \gamma_3^2(-4 + \mu)\mu \\
&- \gamma_3^3(1 + 2\mu) + \gamma_3(-2 - 2\mu + \mu^2)]/[2\gamma_3(1 + \gamma_3)] \ .
\end{aligned} \tag{12}$$

The expressions (12) represent the physical energies at the equilibria. At each of these values, the corresponding collinear equilibria lie on the frontier of the Hill's region, where the motion is allowed. This means that for every energy greater than E_1, E_2, or E_3, the gate at the corresponding equilibria will be opened.

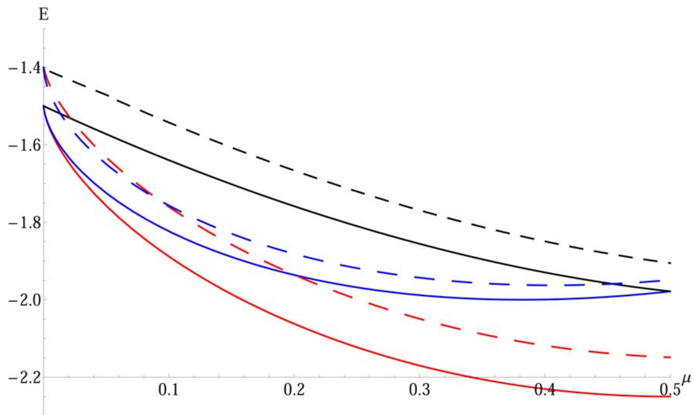

Figure 2: Energy levels at which the gates open at L_1, L_2 and L_3 in red, green and blue respectively, for $\beta = 0$ (continuous lines) and $\beta = 0.1$ (dashed lines).

Figure 2 shows energy levels - as a function of μ - at which the gates open; we report both the results for the case with $\beta = 0$ and $\beta \neq 0$, which are represented, respectively, by continuous and dashed lines.

Figure 3 shows the zero–velocity curves for the cases $\beta = 0$ (continuous lines) and $\beta = 0.1$ (dashed lines). The corresponding energy levels are chosen as those at which the gates of the value $\beta = 0$ open, as shown by the zooms in the cases of L_1 and L_2. We remark that a non-zero value of β might contribute to decrease the energy levels needed to open the gates at the collinear points, giving rise to an earlier exchange between the primaries. Indeed, while the gate for the $\beta = 0$ case is still closed, the Hill's regions for $\beta = 0.1$ allow already the existence of transit orbits. In Figure 3 the (almost overlapping) circles and crosses show the positions of the equilibria for the case $\beta = 0$ and $\beta = 0.1$ respectively.

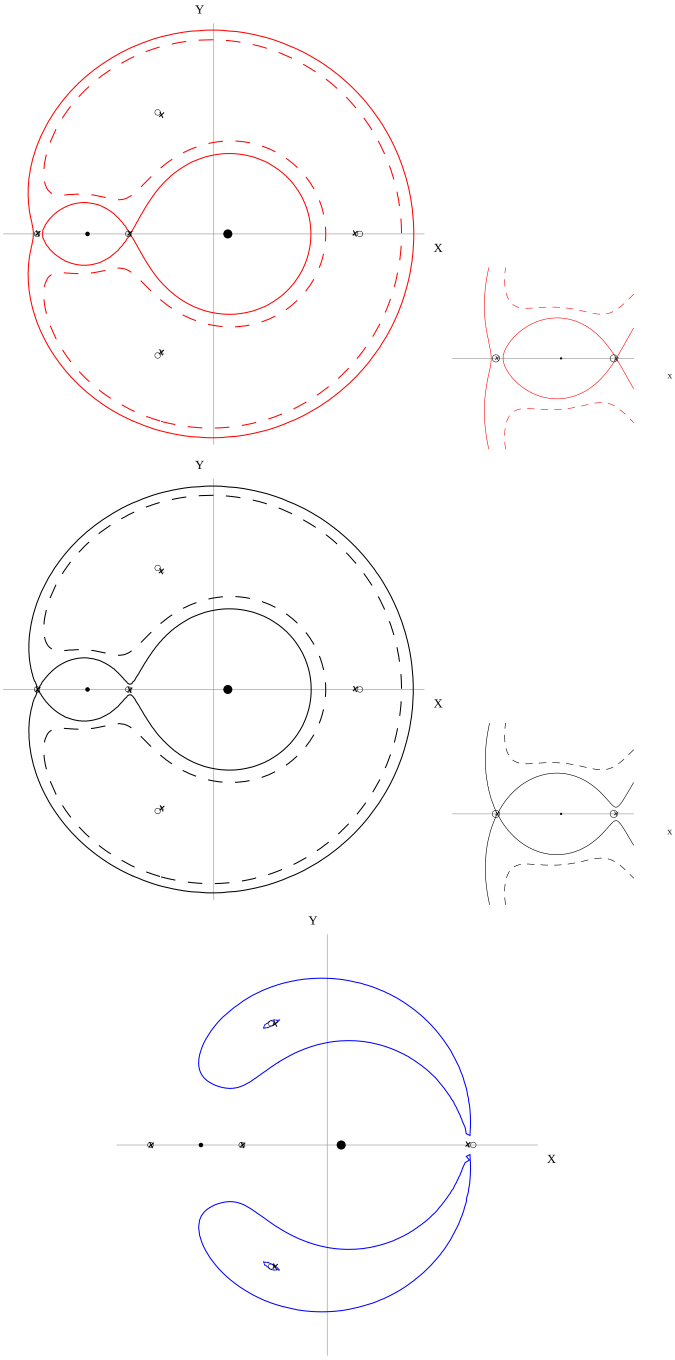

Figure 3: Zero–velocity curves for the cases $\beta = 0$ (continuous line) and $\beta = 0.1$ (dashed line). Upper plots: energy level of L_1 and a zoom on the gate; middle plots: energy level of L_2 and a zoom on the gate; lower plot: energy level of L_3. The positions of the equilibria are given by circles for $\beta = 0$ and crosses for $\beta = 0.1$.

3. Reduction to the center manifold

In this Section we follow the procedure illustrated, e.g. in [2], to reduce the system to the center manifold, thus allowing for the separation of the hyperbolic direction from the other components.

To this end, we transform the system of equations (2) by making a preliminary change of variables, which allows us to scale and shift to one of the collinear equilibria. Precisely, we use the following transformation to the new coordinates (x, y, z) defined by the relations

$$X = \mp\gamma_j x + \mu + a \ , \qquad Y = \mp\gamma_j y \ , \qquad Z = \gamma_j z \ , \tag{13}$$

where the upper signs hold for L_1, L_2, while the lower signs are referred to L_3. Moreover, we set $a = -1 + \gamma_1$ for L_1, $a = -1 - \gamma_2$ for L_2, $a = \gamma_3$ for L_3. Then, we expand the potential Ω in terms of the Legendre polynomials; denoting by $\mathcal{P}_n(\chi)$ the Legendre polynomial of order n and argument χ, and setting $\rho = \sqrt{x^2 + y^2 + z^2}$, we obtain

$$\Omega(x, y, z) = \sum_{n\geq 3} c_n(\mu)\rho^n \ ,$$

where the coefficients $c_n = c_n(\mu)$ are given by

$$\begin{aligned}
c_n(\mu) =& \frac{1}{\gamma_1^3}\left(\mu + (-1)^n \frac{(1-\mu)(1-\beta)\gamma_1^{n+1}}{(1-\gamma_1)^{n+1}}\right) \qquad && \text{for } L_1 \ , \\
c_n(\mu) =& \frac{(-1)^n}{\gamma_2^3}\left(\mu + \frac{(1-\mu)(1-\beta)\gamma_2^{n+1}}{(1+\gamma_2)^{n+1}}\right) && \text{for } L_2 \ , \\
c_n(\mu) =& \frac{(-1)^n}{\gamma_3^3}\left((1-\mu)(1-\beta) + \frac{\mu\gamma_3^{n+1}}{(1+\gamma_3)^{n+1}}\right) && \text{for } L_3 \ .
\end{aligned}$$

We can write the equations of motion (2) as

$$\begin{aligned}
\ddot{x} - 2\dot{y} - (1 + 2c_2)x \quad &= \quad \frac{\partial}{\partial x}\sum_{n\geq 3} c_n(\mu)\rho^n \mathcal{P}_n\left(\frac{x}{\rho}\right) \\
\ddot{y} + 2\dot{x} + (c_2 - 1)y \quad &= \quad \frac{\partial}{\partial y}\sum_{n\geq 3} c_n(\mu)\rho^n \mathcal{P}_n\left(\frac{x}{\rho}\right) \\
\ddot{z} + c_2 z \quad &= \quad \frac{\partial}{\partial z}\sum_{n\geq 3} c_n(\mu)\rho^n \mathcal{P}_n\left(\frac{x}{\rho}\right) \ .
\end{aligned}$$

Denoting by $p_x = \dot{x} - y$, $p_y = \dot{y} + x$, $p_z = \dot{z}$ the momenta conjugated to x, y, z, respectively, we can write the Hamiltonian $H^{(IN)}$ in (5) as

$$H^{(in)}(p_x, p_y, p_z, x, y, z) = \frac{1}{2}\left(p_x^2 + p_y^2 + p_z^2\right) + yp_x - xp_y - \sum_{n\geq 2} c_n(\mu)\rho^n \mathcal{P}_n\left(\frac{x}{\rho}\right) \ . \tag{14}$$

The quadratic part of the Hamiltonian, say $H_2^{(in)}$, is thus of the form:

$$\begin{aligned} H_2^{(in)}(p_x,p_y,p_z,x,y,z) &= \frac{1}{2}\left(p_x^2+p_y^2\right)+yp_x-xp_y-c_2x^2 \\ &+ \frac{c_2}{2}y^2+\frac{p_z^2}{2}+\frac{c_2}{2}z^2\ , \end{aligned} \tag{15}$$

where the coefficient c_2 provides the frequency ω_z of the z-direction, being $\omega_z = \sqrt{c_2}$. Next step consists in reducing the quadratic part to a simpler form. It can be shown that the system associated to (15) admits four eigenvalues (see [11], [2] for full details), say $\pm\sqrt{\eta_1}$ and $\pm\sqrt{\eta_2}$, with

$$\eta_1 = \frac{c_2-2-\sqrt{9c_2^2-8c_2}}{2}\ , \qquad \eta_2 = \frac{c_2-2+\sqrt{9c_2^2-8c_2}}{2}\ .$$

Since $c_2 > 1$, we have $\eta_1 < 0$ and $\eta_2 > 0$, which shows that the equilibrium point is of the type saddle $\times$ center $\times$ center. A symplectic change of variables can thus be found (see [11]), such that the linearised Hamiltonian (15) takes the form

$$H_2^{(d)}(p_1,p_2,p_3,q_1,q_2,q_3) = \lambda_x q_1p_1 + i\omega_y q_2p_2 + i\omega_z q_3p_3 \tag{16}$$

with $\omega_y \equiv \sqrt{-\eta_1}$, $\lambda_x \equiv \sqrt{\eta_2}$ and where we denote the new diagonalising variables as $(p,q) = (p_1,p_2,p_3,q_1,q_2,q_3)$. The explicit derivation of the diagonalising transformation is a standard procedure (see, e.g., Appendix B of [2]); therefore, it will not be included in the present work.

Given the saddle$\times$center$\times$center character of the equilibria, the center manifold reduction consists in focussing the study on the central directions and in eliminating the hyperbolic component. To this aim, we consider the diagonalising change of variables which led to (16) and we implement it on the full Hamiltonian (14); such procedure yields a Hamiltonian of the form

$$H^{(d)}(p_1,p_2,p_3,q_1,q_2,q_3) = \sum_{n\geq 2} H_n^{(d)}(p,q)\ , \tag{17}$$

where $H_2^{(d)}$ is given by (16) and $H_n^{(d)}$ are homogeneous polynomials of degree n. Then, we implement a Birkhoff normalization adapted to the resonance $\omega_y = \omega_z$, which is obtained through a suitable canonical transformation, say $(p,q) \longrightarrow (P,Q)$, generated by means of Lie series.

We investigate the sole $\omega_y = \omega_z$ resonance as for any $\mu \in (0, 1/2]$ the two elliptic frequencies are such that the quantity

$$\delta \equiv \omega_y - \omega_z\ ,$$

to which we refer as the *detuning*, is always a small quantity (in our examples it will be of the order of 10^{-2}).

By Birkhoff normal form it is meant that the Hamiltonian (17) is transformed to the form:

$$
\begin{aligned}
& K^{(NF)}(P_1,P_2,P_3,Q_1,Q_2,Q_3) = \lambda_x Q_1 P_1 + i\omega_y Q_2 P_2 + i\omega_z Q_3 P_3 \\
+ \ & \sum_{n=3}^{N} K_n^{(NF)}(Q_1P_1,P_2,P_3,Q_2,Q_3) + R_{N+1}(P,Q) \ , \qquad (18)
\end{aligned}
$$

where the homogeneous polynomials $K_n^{(NF)}$, $n = 3, ..., N$, are in *normal form* with respect to the (synchronous) resonant quadratic part $K_2^{(NF)} = H_2^{(r)}$, where

$$
H_2^{(r)}(P_1,P_2,P_3,Q_1,Q_2,Q_3) \equiv \lambda_x Q_1 P_1 + i\omega_z (Q_2 P_2 + Q_3 P_3) \ ,
$$

while $R_{N+1}(P,Q)$ is a remainder function of degree $N+1$ in the variables (P,Q). In particular, each term up to order N in the series (18) satisfies the condition

$$
\{H_2^{(r)}, K_n^{(NF)}\} = 0 \ ,
$$

where $\{\cdot,\cdot\}$ denotes the Poisson brackets. Notice that, since the normalization involving the hyperbolic components is a standard Birkhoff normalization, the normal form only depends on Q_1, P_1 through their product, while the remainder $R_{N+1}(P,Q)$ might depend on Q_1, P_1 separately.

Next step consists in complexifying and passing to action–angle variables $(I_x, I_y, I_z, \theta_x, \theta_y, \theta_z)$ by means of the following transformation:

$$
\begin{cases}
Q_1 = \sqrt{I_x} e^{\theta_x} \\
Q_2 = -i\sqrt{I_y} e^{i\theta_y} \\
Q_3 = -i\sqrt{I_z} e^{i\theta_z} \\
P_1 = \sqrt{I_x} e^{-\theta_x} \\
P_2 = \sqrt{I_y} e^{-i\theta_y} \\
P_3 = \sqrt{I_z} e^{-i\theta_z} \ .
\end{cases}
$$

The resulting Hamiltonian is finally reduced to the dynamics on the center manifold by setting the initial condition of the action $I_x = Q_1 P_1$ to zero and neglecting the remainder R_{N+1}. In this way we obtain an integrable, 2-DOF Hamiltonian function, which provides the dynamics in the center manifold up to an approximation of order N.

In fact, the resulting Hamiltonian takes the form:

$$
K^{(CM)}(I_y, I_z, \theta_y, \theta_z) = \sum_{n=0}^{N} K_n^{(CM)}(I_y, I_z, \theta_y - \theta_z) \ ,
$$

where $K_n^{(CM)} = 0$ for all n odd, while, up to fourth order, it results:

$$\begin{aligned}
K_0^{(CM)}(I_y, I_z) &= \omega_y I_y + \omega_z I_z \\
K_2^{(CM)}(I_y, I_z, \theta_y - \theta_z) &= \alpha I_y^2 + \tilde{\beta} I_z^2 + I_y I_z (\sigma + 2\tau \cos(2(\theta_y - \theta_z))) \\
K_4^{(CM)}(I_y, I_z, \theta_y - \theta_z) &= \alpha_{3300} I_y^3 + \alpha_{0033} I_z^3 + \alpha_{1122} I_y I_z^2 \\
&+ \alpha_{2211} I_y^2 I_z + 2 I_y I_z [\alpha_{2013} I_z + \alpha_{3102} I_y] \cos(2(\theta_y - \theta_z))
\end{aligned}$$

for suitable coefficients α, $\tilde{\beta}$, σ, τ and α_{abcd} with $a + b + c + d = 6$. The Hamiltonian $K^{(CM)}(I_y, I_z, \theta_y, \theta_z)$ is an *integrable* one since, by construction,

$$\mathcal{E} = I_y + I_z$$

is a second integral of motion and provides an approximation of the dynamics of the system (14) at the scaled energy level $H^{(in)} = E$.

4. The bifurcation thresholds under SRP

As we mentioned in Section 1, we compute the bifurcations of just L_1 and L_2. In fact, the case of L_3 is rather peculiar, since the effect of the smaller primary is almost negligible and the model is close to a Kepler's problem. Indeed, for this reason, as shown in [3], the normal form turns out to be inadequate to study the bifurcation thresholds when the mass ratio of the primaries is smaller than 10^{-2} (we refer to [3] for further details). Therefore, the Earth-Moon system is, more or less, a limit case and the Sun-Earth L_3 location is far from a reliable description.

We start by recalling the expressions of the bifurcation thresholds derived in [2] and [3]. Precisely, the following quantities provide the first-order estimates of the thresholds ensuring the existence of resonant orbits, bifurcating from the normal modes:

$$\begin{aligned}
\mathcal{E}_{\ell y}^{(1)} &= \frac{\delta}{\sigma - 2(\alpha + \tau)} \\
\mathcal{E}_{iy}^{(1)} &= \frac{\delta}{\sigma - 2(\alpha - \tau)} \\
\mathcal{E}_{iz}^{(1)} &= \frac{\delta}{2(\tilde{\beta} - \tau) - \sigma} \\
\mathcal{E}_{\ell z}^{(1)} &= \frac{\delta}{2(\tilde{\beta} + \tau) - \sigma} \ .
\end{aligned} \tag{19}$$

In these expressions, the quantities $\mathcal{E}_{\ell y}^{(1)}$, $\mathcal{E}_{\ell z}^{(1)}$ refer to bifurcations of the halo families, namely the loop orbits satisfying the fixed phase relation $\theta_y - \theta_z = \pm\pi/2$, while $\mathcal{E}_{iy}^{(1)}$, $\mathcal{E}_{iz}^{(1)}$ refer to the *anti–halo* families, namely the inclined orbits satisfying the fixed phase relation $\theta_y - \theta_z = 0$ or $\theta_y - \theta_z = \pi$. The second subscript in (19) refers to which Lyapunov orbit the bifurcation is associated to: y stands for the planar one, while z stands for the vertical one. Notice that to first order in the detuning, the relation between the value of the second integral $\mathcal{E}$ in (19) and the scaled energy E is given by $E = \omega_z \mathcal{E}$.

By using the following second order expressions for the scaled energies of the normal modes

$$E = (\omega_z + \delta)\mathcal{E} + \alpha \mathcal{E}^2 \ , \qquad E = \omega_z \mathcal{E} + \tilde{\beta}\mathcal{E}^2 \ ,$$

the bifurcation thresholds at second order in the detuning are given by the following expressions [13]:

$$E^{(2)}_{\ell y} = \omega_z \left(\mathcal{E}^{(1)}_{\ell y} + \delta^2 \left(\frac{\sigma - \alpha - 2\tau}{(\sigma - 2(\alpha + \tau))^2} - \frac{\alpha_{2211} - 3\alpha_{3300} - \alpha_{3102}}{(\sigma - 2(\tau + \alpha))^3} \right) \right) \ ,$$

$$E^{(2)}_{iy} = \omega_z \left(\mathcal{E}^{(1)}_{iy} + \delta^2 \left(\frac{\sigma - \alpha + 2\tau}{(\sigma - 2(\alpha - \tau))^2} - \frac{\alpha_{2211} - 3\alpha_{3300} + \alpha_{3102}}{(\sigma - 2(\alpha - \tau))^3} \right) \right) \ ,$$

$$E^{(2)}_{iz} = \omega_z \left(\mathcal{E}^{(1)}_{iz} + \delta^2 \left(\frac{\tilde{\beta}}{(\sigma - 2(\tilde{\beta} - \tau))^2} - \frac{\alpha_{1122} - 3\alpha_{0033} + \alpha_{2013}}{(\sigma - 2(\tilde{\beta} - \tau))^3} \right) \right) \ ,$$

$$E^{(2)}_{\ell z} = \omega_z \left(\mathcal{E}^{(1)}_{\ell z} + \delta^2 \left(\frac{\tilde{\beta}}{(\sigma - 2(\tau + \tilde{\beta}))^2} - \frac{\alpha_{1122} - 3\alpha_{0033} - \alpha_{2013}}{(\sigma - 2(\tau + \tilde{\beta}))^3} \right) \right) \ .$$

We observe that, in the purely gravitational case, this full bifurcation sequence is practically never observed. After the first one (the halo at $E_{\ell y}$), which occurs at low energy, only the second bifurcation (the anti-halo at E_{iy}) is reported in some cases at quite high energy: we recall e.g. the accurate numerical investigation by Gomez and Mondelo in [9] of the Earth-Moon system. The ensuing anti-halo families are unstable and their birth is accompanied by the return to stability of the planar Lyapunov orbit. The third bifurcation is, on the other hand, very interesting: it is actually the *annihilation* at E_{iz} of the anti-halo families on the *vertical* Lyapunov which, at the same time, becomes unstable. Finally, there can be also the remote possibility of the annihilation at $E_{\ell z}$ of the halo families on the vertical Lyapunov which regains stability.

In this approach, the advantage of using the scaled energy E is that, with it, some features of the problem, like the dependency of the thresholds with respect to the parameters μ and β, are better highlighted. However, we must remind that the scaled energy E, namely $H^{(in)}$ in (14), is related to the physical one, say h, namely $H^{(IN)} = h$ in (5), by the following expressions, which are obtained by using the transformations (13):

$$h = E\ \gamma_1^2 - \frac{1}{2}(1 - \gamma_1 - \mu)^2 - \frac{\mu}{\gamma_1} - \frac{1-\mu}{1-\gamma_1} \tag{20}$$

for L_1, and

$$h = E\ \gamma_2^2 - \frac{1}{2}(1 + \gamma_2 - \mu)^2 - \frac{\mu}{\gamma_2} - \frac{1-\mu}{1+\gamma_2} \tag{21}$$

for L_2.

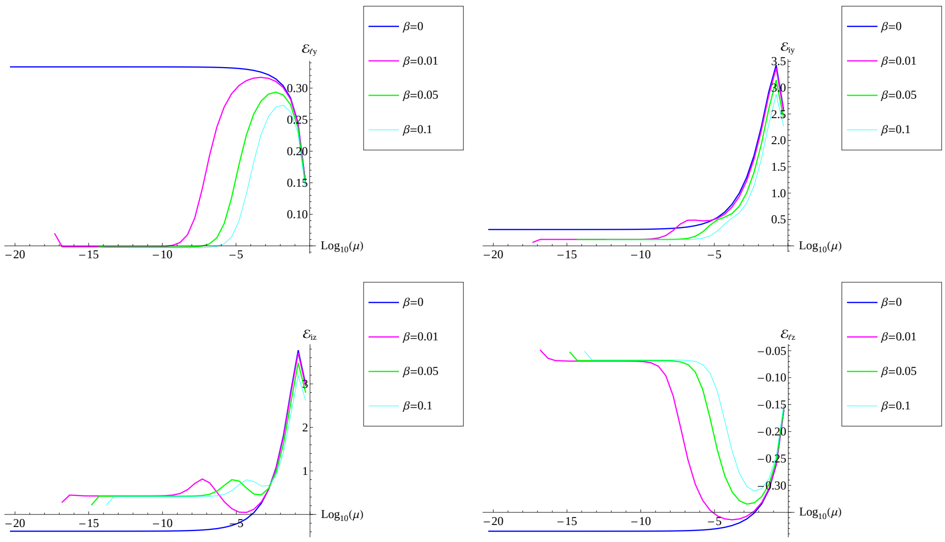

Figure 4: Equilibrium point L_1: $E_{\ell y}$ (top left), E_{iy} (top right), E_{iz} (bottom left), $E_{\ell z}$ (bottom right).

The values of the four bifurcation thresholds for L_1 and L_2 are shown in Figures 4 and 5, respectively; we provide such values for the mass ratio ranging from 0 to $\frac{1}{2}$ and the parameter β taking the values $\beta = 0$, 0.01, 0.05, 0.1.

For L_1 we can see that both the second and, remarkably, the third bifurcations are predicted to occur for $\mu < 10^{-4}$ at moderate values of the scaled energy. For L_2 instead the corresponding predictions are at very high scaled energies, making these bifurcations practically impossible. In both cases the fourth bifurcation can never occur.

As already remarked, we stress that the energy displayed in these figures is not the physical one, which is instead shown in Figures 6 and 7 by using (20)-(21). Such figures provide the results for the physical energy of the system in a logarithmic scale, for mass ratios such that $\mu < 10^{-4}$ and $\mu \geq 10^{-4}$.

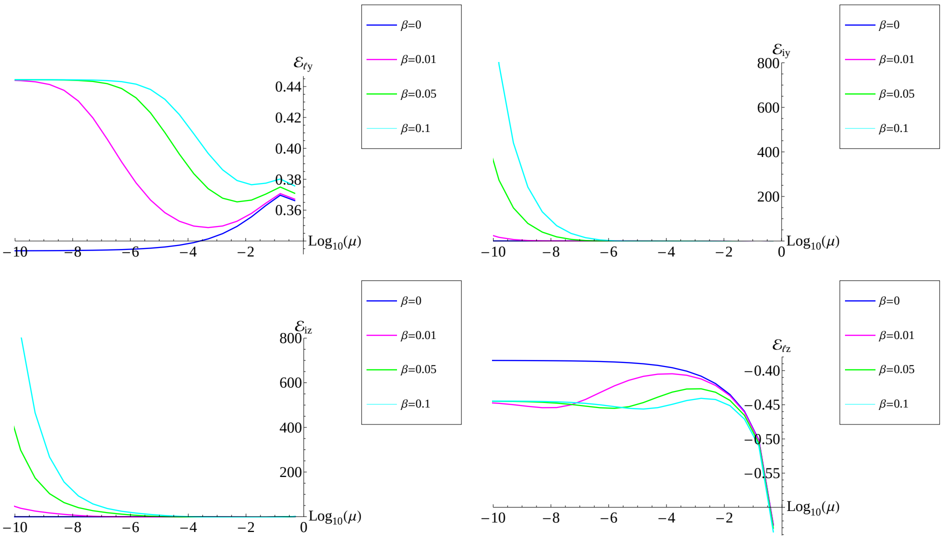

Figure 5: Equilibrium point L_2: $E_{\ell y}$ (top left), E_{iy} (top right), E_{iz} (bottom left), $E_{\ell z}$ (bottom right).

5. Conclusions

The results presented in this paper show that the effect of solar radiation pressure might be relevant for the dynamics of the collinear points L_1 and L_2. Beside provoking a (slight) displacement in the location of the equilibria, solar radiation pressure modifies the values of the energy thresholds at which one has the bifurcation of the halo and anti-halo orbits.

The magnitude of such effect depends also on the mass parameter. In particular, we notice that for $\mu \geq 10^{-4}$ the introduction of the solar radiation pressure does not significantly affect the bifurcation threshold; this case applies for example to Jupiter-size bodies.

However, from the analysis of Figures 6 and 7, it is clear that in the limit of smaller μ, the thresholds of the bifurcations at L_1 and L_2 tend to the same energy, as expected. Conceivably, the thresholds for L_1 are more affected than those for L_2. Finally, we observe that using $\beta \neq 0$ does not always lower the thresholds corresponding to the different bifurcations.

References

[1] C. Howell, B. T. Barden, M. Lo, *Application of dynamical systems theory to trajectory design for a libration point mission,* The Journal of the Astronautical Sciences **45**, Issue 2, 161-178 (1997)

[2] S. Bucciarelli, M. Ceccaroni, A. Celletti, G. Pucacco, *Qualitative and analytical results of the bifurcation thresholds to halo orbits*, "Annali di

Matematica Pura ed Applicata", $http://dx.doi.org/10.1007/s10231-015-0474-2$ (2015)

[3] M. Ceccaroni, A. Celletti, G. Pucacco, *Halo orbits around the collinear points of the restricted three-body problem*, submitted to Physica D (2015)

[4] A. Celletti, *Stability and Chaos in Celestial Mechanics*, Springer-Verlag, Berlin; published in association with Praxis Publishing Ltd., Chichester, ISBN: 978-3-540-85145-5 (2010)

[5] A. Celletti, G. Pucacco, D. Stella, *Lissajous and Halo orbits in the restricted three-body problem*, J. Nonlinear Science **25**, Issue 2, 343-370 (2015)

[6] L. Euler, *Considerationes de motu corporum coelestium.* Novi commentarii academiae scientiarum Petropolitanae **10**, 544-558 (1764) (read at Berlin in 1762). See also: *Opera Omnia,* s. 2, **25**, 246-257

[7] A. Farrés, A. Jorba, *Station keeping of a solar sail around a Halo orbit,* Acta Astronautica **94**, Issue 1, 527-539 (2014)

[8] A. Farrés, A. Jorba, J-M. Mondelo, *Orbital dynamics for a non-perfectly reflecting Solar sail close to an asteroid,* Proceedings of the 2nd IAA Conference on Dynamics and Control of Space System, Rome, Italy, 24-26 March 2014

[9] G. Gómez, J.M. Mondelo, *The dynamics around the collinear equilibrium points of the RTBP,* Physica D **157**, 283-321 (2001)

[10] M. Hénon, *Vertical stability of periodic orbits in the restricted problem. I. Equal masses,* Astron. & Astrophys. **28**, 415-426 (1973)

[11] À. Jorba, J. Masdemont, *Dynamics in the center manifold of the collinear points of the restricted three body problem,* Physica D **132**, 189-213 (1999)

[12] J.-L. Lagrange, *Essai sur le problème des trois corps,* Prix de l'Académie royale des sciences de Paris, tome IX (1772)

[13] A. Marchesiello, G. Pucacco, *Universal unfolding of symmetric resonances,* Celestial Mechanics and Dynamical Astronomy, **119**, 357–368 (2014).

[14] C. R. McInnes, *Solar Sailing: Technology, Dynamics and Mission Applications*, Springer Praxis Books / Astronomy and Planetary Sciences (2004)

[15] C.D. Murray, S.F. Dermott, *Solar system dynamics*, Cambridge University Press (1999)

[16] D. L. Richardson, *Analytic construction of periodic orbits about the collinear points*, Celestial Mechanics **22**, 241-253 (1980)

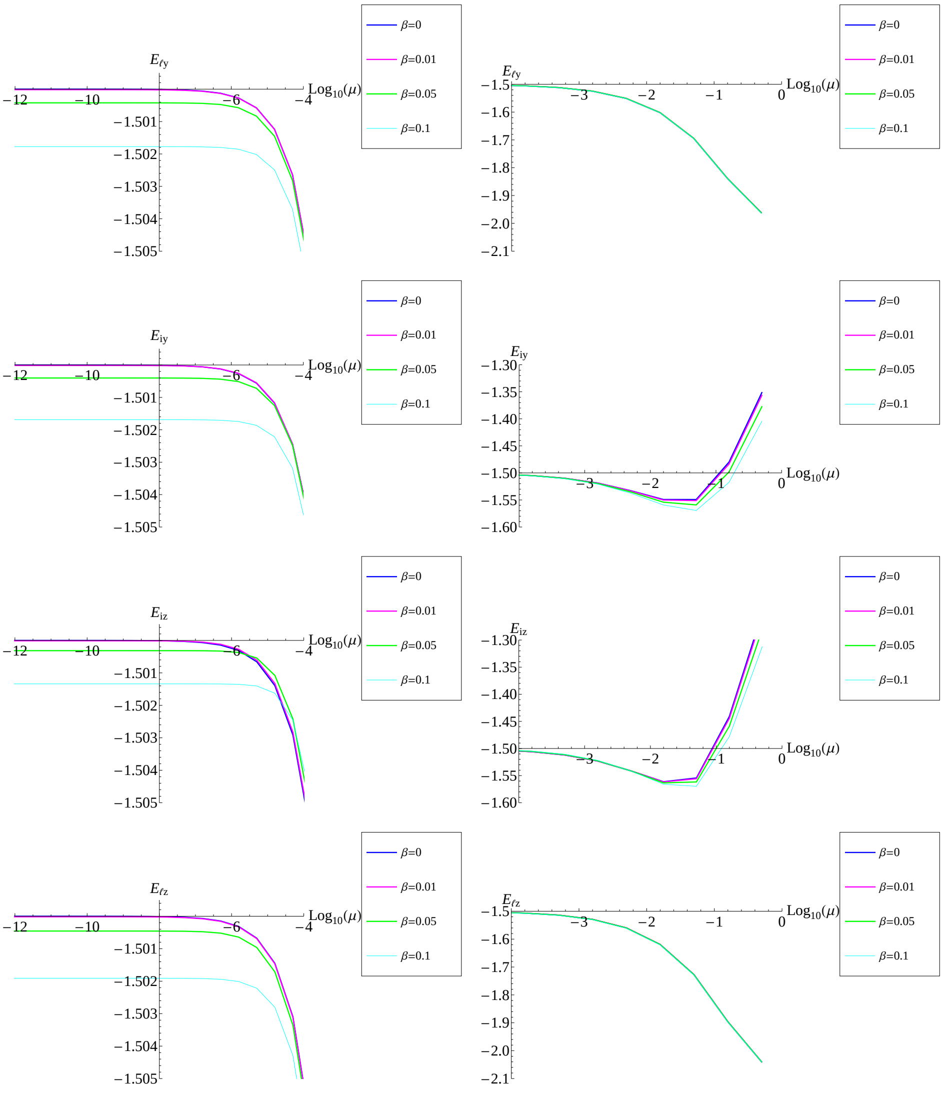

Figure 6: Equilibrium point L_1, physical energy: $h_{\ell y}$,h_{iy},h_{iz},$h_{\ell z}$. Left: $\mu < 10^{-4}$, right: $\mu \geq 10^{-4}$.

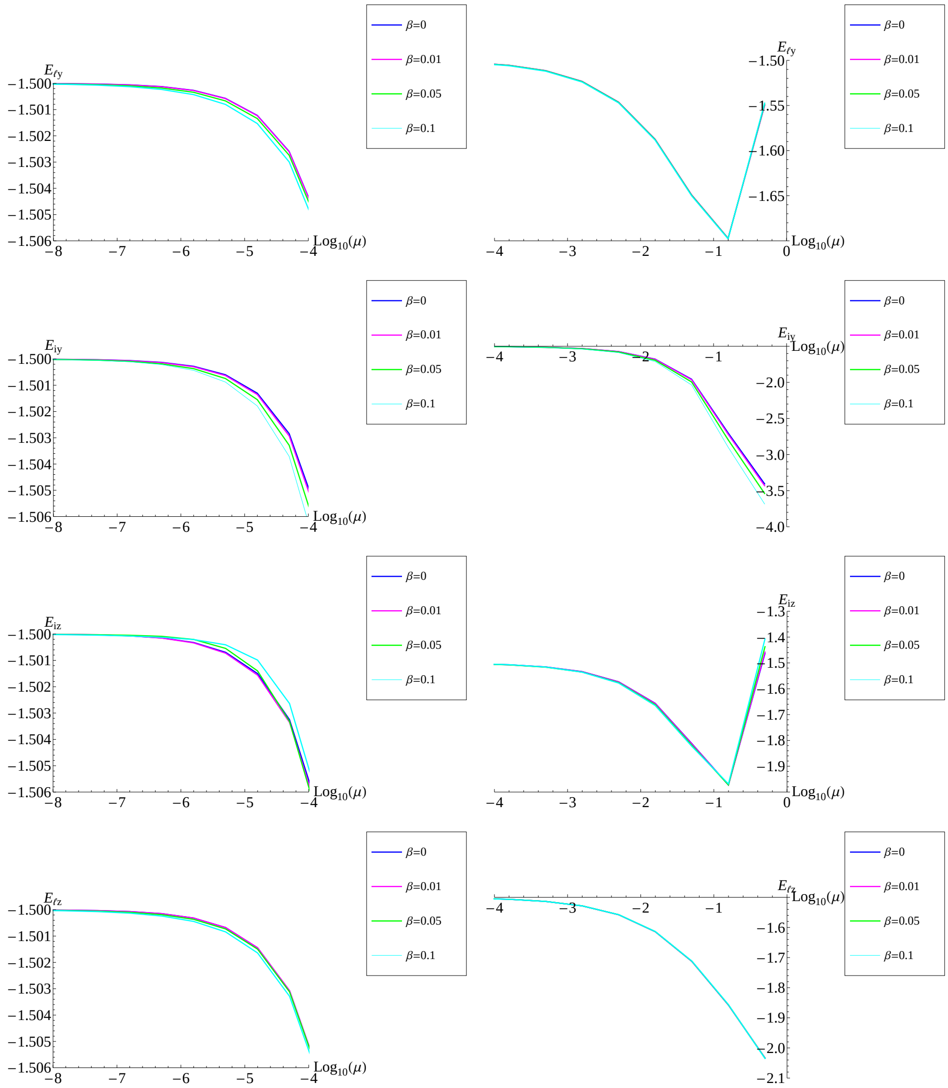

Figure 7: Equilibrium point L_2, physical energy: $h_{\ell y}$,h_{iy},h_{iz},$h_{\ell z}$. Left: $\mu < 10^{-4}$, right: $\mu \geq 10^{-4}$.